Proceedings of the 14th Asian Control Conference
July 5-8, 2024, Dalian, China

An Adaptive Model Predictive Control for Unmanned Underwater Vehicles Subject to External Disturbances and Measurement Noise

Li-Yu Lo[1*] *Student Member, IEEE*, Yang Hu[1*] , Boyang Li[2], Chih-Yung Wen[1], and Yefeng Yang[1†]

***Abstract*— This research addresses the trajectory tracking problem of an unmanned underwater vehicle (UUV) within 4 degrees of freedom (DOF) subject to external disturbances and measurement noise. An adaptive control framework consisting of an adaptive model predictive control (MPC) and an error-state extended state observer (ESESO) is proposed. The MPC is utilized to stabilize the system while the ESESO is proposed to estimate the disturbances. In contrast to most conventional ESOs, we explicitly formulate a sensor-fusion problem by tracking the error state of the observer. The ESESO feeds back the filtered state and the estimated lump disturbances to the MPC to achieve the adaptability of the closed-loop system. Sufficient simulation via a semi-physical experiment is conducted to validate the effectiveness and superiority of the proposed control framework.**

***Index Terms*— Unmanned Underwater Vehicles, Trajectory Tracking, Error-State Extended State Observer, Adaptive Model Predictive Control.**

I. INTRODUCTION

Recently, unmanned underwater vehicles (UUVs) have garnered substantial attention from both the academia and the industry. Providing a promising alternative solution to replace human operators, UUVs showcase their unprecedented applicability in various scenarios [1], [2], [3], [4]. However, UUVs still fall short of achieving full autonomy and current practices often require human-in-the-loop [5], [6] technique to guarantee the success of missions, particularly in addressing uncertainties in motion control. Therefore, the control problem of UUVs needs to be further investigated.

Several significant works have been proposed to solve the UUV control problem. In [7], a vision-based neural network controller was proposed to stabilize the heave of a UUV. Zhao et al. [8] utilized fault tolerant-based MPC to achieve trajectory control of a UUV. A sliding mode-based control method was utilized in reference [9] for the UUV dynamic base recovery problem. A fractional-order recurrent neural network-based control framework was investigated in a Multi-UUV manoeuvring counter-game scenario. Among the various control methods mentioned above, MPC is widely employed due to its simple structure and capability to consider multiple constraints.

MPC is one of the most commonly adopted controllers in the field of robotics, where platforms such as fixed-wing aerial robots [10] or ground vehicles [11] frequently utilize the control technique to perform trajectory manoeuvres. Specifically, MPC operates iteratively by addressing an optimal control problem over a finite time horizon, allowing it to generate optimal control inputs based on the system's dynamic model and constraints. However, MPC's excessive reliance on precise system models impedes its further development.

Many scholars have conducted in-depth research on reducing the model dependency of MPC. A disturbance rejection MPC framework was introduced in [12] for a class of input-affine nonlinear systems. In [13], an event-based robust MPC method was proposed for distributed nonlinear discrete systems. Another innovative event-based work was proposed in [14], which addressed control problems of a class of Markovian jump systems with disturbances. Specifically, some recently published work provided some UUV applications based on robust MPC. For example, in [15], an MPC approach was put forward for the real-time obstacle avoidance of a UUV. An extended Kalman filter (EKF) based MPC was employed for trajectory tracking of a UUV with disturbances [16].

The analysis aforementioned indicates the combination of the MPC and the disturbance observers is frequently adopted for UUVs. Nevertheless, it could be seen that most research are done under an ideal environment where real-world deploying situations are not considered, i.e., physical sensor models and the corresponding measurement noises are not included. Therefore, we design an extended state observer (ESO) based on inertial measurement units (IMU) to establish the groundwork for future practical applications. Meanwhile, as tracking the state with error-state provides a better linearization property [17], here, the error-state extended state observer (ESESO) is proposed.

The contributions are listed as follows:

- An adaptive nonlinear MPC is presented for UUV, where the prediction model is integrated with an ESESO that could be directly applied to real sensor models.
- An inertial-based sensor fusion scheme is proposed to design the ESESO. The framework intakes the IMU and any arbitrary exteroceptive sensor model to conduct both state estimation and disturbance observation.
- The modules are integrated and validated via a semi-physical experiment. The details[1] are also released for

∗ The authors contributed equally.

[1]Li-Yu Lo, Yang Hu, Chih-Yung Wen and Yefeng Yang are with AIRo-LAB, Department of Aeronautical and Aviation Engineering, The Hong Kong Polytechnic University, Kowloon, Hong Kong (e-mail: patty.lo@connect.polyu.hk; yang-h.hu@connect.polyu.hk; chi-hyung.wen@polyu.edu.hk; yefeng.yang@connect.polyu.hk).

[2]Boyang Li is with School of Engineering, The University of Newcastle, Callaghan, NSW 2308, Australia (e-mail: boyang.li@newcastle.edu.au).

† Corresponding author

[1]https://github.com/HKPolyU-UAV/bluerov2

future research.

The remaining sections of this paper are structured as follows: section II describes the UUV dynamic model; section III elucidates the ESESO with EKF. The MPC is successively formulated in section IV. In section V, the simulation results are presented. Finally, section VI concludes this paper.

In what follows, $\mathcal{I}$ and $\mathcal{B}$ denote the inertial and body frame, respectively. $\boldsymbol{\eta}_{\mathcal{I}} = [x, y, z, \phi, \theta, \psi]^\top \in \mathbb{R}^6$ is the generalized position vector in $\mathcal{I}$ with $[x, y, z]$ and $[\phi, \theta, \psi]$ be the position and attitude of the UUV. $\mathbf{v}_{\mathcal{B}} = [u, v, w, p, q, r]^\top \in \mathbb{R}^6$ is the generalized velocity vector with $\mathbf{v}_{T,\mathcal{B}} = [u, v, w]$ be the linear velocity and $\mathbf{v}_{R,\mathcal{B}} = [p, q, r]$ be the angular velocity. $\mathbf{K} \in \mathbb{R}^{6\times6}$ is the propulsion matrix, $\mathbf{A} \in \mathbb{R}^{6\times4}$ is the control allocation matrix, and both $\mathbf{K}$ and $\mathbf{A}$ are constant matrices. m is the mass, and $\mathbf{I}_m = [I_{m,x}, I_{m,y}, I_{m,z}]$ is the moment of inertial of 3 axis, and z_{CG} is the z-axis component of the centre of gravity position within the body frame. $\mathbf{m} \in \mathbb{R}^6$ is the added mass vector, with $\mathbf{m}_T \in \mathbb{R}^3$ be the translational term and $\mathbf{m}_R \in \mathbb{R}^3$ the rotational term. g is the gravity constant. $C\cdot$, $S\cdot$, and $T\cdot$ are the cosine, sine, and tangent functions, respectively. $\circ$ is the Hadamard product operator. $[\cdot]_\times$ is the skew-symmetric matrix of a vector.

II. UUV Dynamics Model

In this work, we adopt the open-frame BlueROV2 vehicle [18], which encompasses 4-DoF of motion, say, surge, sway, heave, and yaw. We employ Fossen's theory [19] to model the nonlinear dynamics of the UUV.

The dynamics of the UUV is given by

$$\begin{aligned} \dot{\mathbf{x}} &= \begin{bmatrix} \dot{\boldsymbol{\eta}}_{\mathcal{I}} \\ \dot{\mathbf{v}}_{\mathcal{B}} \end{bmatrix} = \begin{bmatrix} \mathbf{J}_\Theta \mathbf{v}_{\mathcal{B}} \\ \mathbf{M}^{-1}\left(\boldsymbol{\tau}_{\mathcal{B}} + \boldsymbol{\xi}_{\mathcal{B}} + \mathbf{S}\right) \end{bmatrix} = \mathbf{F}(\mathbf{x}, \boldsymbol{\tau}_{\mathcal{B}}) \\ \boldsymbol{\tau}_{\mathcal{B}} &= \mathbf{KAU} \in \mathbb{R}^4 \\ \mathbf{S} &= -\mathbf{C}(\mathbf{v}_{\mathcal{B}})\mathbf{v}_{\mathcal{B}} - \mathbf{D}(\mathbf{v}_{\mathcal{B}})\mathbf{v}_{\mathcal{B}} - \mathbf{g}(\boldsymbol{\eta}_{\mathcal{I}}) \in \mathbb{R}^6. \end{aligned} \tag{1}$$

In particular, $\mathbf{J}_\Theta = \begin{bmatrix} \mathbf{R}_\Theta & \mathbf{0}_{3\times3} \\ \mathbf{0}_{3\times3} & \mathbf{T}_\Theta \end{bmatrix} \in \mathbb{R}^{6\times6}$ is the coordinate transformation matrix with

$$\mathbf{R}_\Theta = \begin{bmatrix} C\psi C\theta & C\psi S\theta S\phi - S\psi C\phi & C\psi S\theta C\phi + S\psi S\phi \\ S\psi C\theta & S\psi S\theta S\phi + C\psi C\phi & S\psi S\theta C\phi - C\psi S\phi \\ -S\theta & C\theta S\phi & C\theta C\phi \end{bmatrix},$$

and

$$\mathbf{T}_\Theta = \begin{bmatrix} 1 & S\phi T\theta & C\phi T\theta \\ 0 & C\phi & -S\phi \\ 0 & \frac{S\phi}{C\theta} & \frac{C\phi}{C\theta} \end{bmatrix}.$$

$\mathbf{M} = \mathbf{M}_{RB} + \mathbf{M}_A$ is the mass matrix with

$$\mathbf{M}_{RB} = \begin{bmatrix} m & 0 & 0 & 0 & mz_g & 0 \\ 0 & m & 0 & -mz_g & 0 & 0 \\ 0 & 0 & m & 0 & 0 & 0 \\ 0 & -mz_g & 0 & I_{m,x} & 0 & 0 \\ mz_g & 0 & 0 & 0 & I_{m,y} & 0 \\ 0 & 0 & 0 & 0 & & I_{m,z} \end{bmatrix}$$

be the rigid body mass matrix and $\mathbf{M}_A = \text{diag}[\mathbf{m}_A]$ be the added mass matrix. $\boldsymbol{\tau}_{\mathcal{B}}$ is the combined propulsion forces and moments, $\boldsymbol{\xi}_{\mathcal{B}}$ is the lump disturbances, and $\mathbf{U} \in \mathbb{R}^4$ is the control input.

$\mathbf{C}(\cdot)$, $\mathbf{D}(\cdot)$, and $\mathbf{g}(\boldsymbol{\eta}_{\mathcal{I}})$ are the terms related to Coriolis and centripetal forces, hydrodynamic damping force and hydrostatic restoring force.

$$\begin{aligned} \mathbf{C}(\mathbf{v}_{\mathcal{B}}) &= \mathbf{C}_{RB}(\mathbf{v}_{\mathcal{B}}) + \mathbf{C}_A(\mathbf{v}_{\mathcal{B}}) \\ &= \begin{bmatrix} \mathbf{0}_{3\times3} & [-m\mathbf{v}_{T,\mathcal{B}}]_\times \\ [-m\mathbf{v}_{T,\mathcal{B}}]_\times & [-\mathbf{I}_m \circ \mathbf{v}_{R,\mathcal{B}}]_\times \end{bmatrix} \\ &\quad + \begin{bmatrix} \mathbf{0}_{3\times3} & [\mathbf{m}_T \circ \mathbf{v}_{T,\mathcal{B}}]_\times \\ [\mathbf{m}_T \circ \mathbf{v}_{T,\mathcal{B}}]_\times & [\mathbf{m}_R \circ \mathbf{v}_{R,\mathcal{B}}]_\times \end{bmatrix}, \end{aligned} \tag{2}$$

where $\mathbf{C}_{RB}(\mathbf{v}_{\mathcal{B}})$ is the rigid body dynamics and $\mathbf{C}_A(\mathbf{v}_{\mathcal{B}})$ is the added mass dynamics.

$$\begin{aligned} \mathbf{D}(\mathbf{v}_{\mathcal{B}}) &= \mathbf{D}_{RB} + \mathbf{D}_A(\mathbf{v}_{\mathcal{B}}) \\ &= -\text{diag}[\mathbf{d}_L] - \text{diag}[\mathbf{d}_{NL} \circ |\mathbf{v}_{\mathcal{B}}|], \end{aligned} \tag{3}$$

where $\mathbf{d}_L$, $\mathbf{d}_{NL} \in \mathbb{R}^6$ are respectively the linear and nonlinear damping parameter vectors.

$$\mathbf{g}(\boldsymbol{\eta}_{\mathcal{I}}) = \begin{bmatrix} (W-B)S\theta \\ -(W-B)C\theta S\phi \\ -(W-B)C\theta S\phi \\ z_{CG}WC\theta S\phi \\ z_{CG}WS\theta \\ 0 \end{bmatrix} \tag{4}$$

with $W = mg$ be the weight and B be the buoyancy.

From above, $\mathbf{x}$ and $\boldsymbol{\xi}_{\mathcal{B}}$ are needed to be estimated by the ESESO. $\boldsymbol{\tau}_{\mathcal{B}}$ is acquired from the measurements. The rest of the parameters are then determined via offline system identification.

III. Error-State Extended State Observer

This section establishes a loosely coupled sensor fusion-based ESESO to accurately track the state and the lump disturbances with measurement noise.

A. Observer Formulation

The proposed observer is a variation of ESO, where the general problem formulation can be seen in [20]. Here, we apply an adaptive observer gain as in [21], while making the tracking state lie within the error state space. In addition, considering that the observer proposed in this study is conducted with the manifold theory, some notations are made to avoid misunderstandings. The observer state is first defined as

$$\mathbf{z} = \begin{bmatrix} \mathbf{p} & \mathbf{v} & \mathbf{R}_\Theta & \mathbf{b}_a & \mathbf{b}_g & \mathbf{g}_{\mathcal{I}} & \boldsymbol{\xi} \end{bmatrix} \in \mathcal{M}, \tag{5}$$

where $\mathcal{M} = \mathbb{R}^6 \times \mathbb{SO}(3) \times \mathbb{R}^{12}$ is a Lie group $(\mathcal{M}, \cdot)$, which represents the group set. $\cdot$ denotes the group operation. $\mathbf{p} \in \mathbb{R}^3$ and $\mathbf{v} \in \mathbb{R}^3$ are the translation and translational velocity defined in $\mathcal{I}$, respectively. $\mathbf{b}_a \in \mathbb{R}^3$ and $\mathbf{b}_g \in \mathbb{R}^3$ are accelerometer and gyroscope bias defined in $\mathcal{B}$, $\mathbf{g}_{\mathcal{I}} = [0, 0, g]$ is the gravity vector, and $\boldsymbol{\xi}$ is the translational lump disturbances. $\boxplus$ operation on this manifold is defined as

$$\begin{aligned} &\boxplus : \mathcal{M} \boxplus \mathfrak{m} \to \mathcal{M}, \\ &\text{s.t. } \mathbf{A} \boxplus \Delta = \mathbf{A} \cdot \mathbf{Exp}(\Delta), \mathbf{A} \in \mathcal{M}, \Delta \in \mathbb{R}^n, \end{aligned} \tag{6}$$

where $\mathfrak{m}$ is the tangent space of $\mathcal{M}$, and n is dependent to the DoF of the manifold, and $\mathbf{Exp}(\cdot)$ is the exponential mapping from the tangent space of $\mathcal{M}$ to $\mathcal{M}$. For the terms of $\mathbf{z}$ that lie in vector space, $\mathbf{A} \boxplus \Delta$ is equivalent to $\mathbf{A} + \Delta$, implying that the exponential mapping is identity mapping for them. Contrarily, for $\mathbf{R}_\Theta \in \mathbb{SO}(3)$, the exponential mapping is defined as

$$\begin{aligned}\mathbf{Exp}(\boldsymbol{\theta}) &= \mathbf{exp}([\boldsymbol{\theta}]_\times) = \sum_{n=0}^{\infty} \frac{1}{n!}([\boldsymbol{\theta}]_\times)^n \\ &= C\theta\mathbf{I} + (1 - C\theta)\mathbf{a}\mathbf{a}^\top + S\theta[\mathbf{a}]_\times, \end{aligned} \tag{7}$$

where $\boldsymbol{\theta} = \theta\mathbf{a}$, and $\mathbf{a}$ is the normalized unit vector in $\mathbb{R}^3$. Based on the above, $\boxminus$ operation is defined as

$$\begin{aligned} &\boxminus : \mathcal{M} \boxminus \mathcal{M} \to \mathfrak{m}, \\ \text{s.t. } &\mathbf{A} \boxminus \mathbf{B} = \mathbf{Log}(\mathbf{B}^{-1} \circ \mathbf{A}) = \Delta, \mathbf{A}, \mathbf{B} \in \mathcal{N}, \Delta \in \mathbb{R}^n, \end{aligned} \tag{8}$$

where $\mathbf{Log}(\cdot)$ is the inverse mapping of $\mathbf{Exp}(\cdot)$.

The ESESO tracks the dynamics of the error state, making the observer carry two state parameters, say, the nominal state and the error state. Using the EKF, the error state is filtered, whereas the nominal state receives the estimated error to update. Hence, the error state can be extracted from below, where the true state $\mathbf{z}_t$ comprises nominal state $\mathbf{z}$ and error state $\delta\mathbf{z}$

$$\mathbf{z}_t = \mathbf{z} \boxplus \delta\mathbf{z}. \tag{9}$$

The error term $\delta\mathbf{z}$ lies within the tangent space $\mathfrak{m}$. The tracked error state $\delta\mathbf{z}$ is assumed to be Gaussian, i.e., $\delta\mathbf{z} \sim \mathcal{N}(\mathbf{0}, \mathbf{P})$ with $\mathbf{P}$ be the local perturbations of the $\mathcal{M}$ around $\mathbf{0}$.

Based on the definitions here, the ESESO processes the input signals from sensors along with the states from the previous time step $k-1$ and outputs the error state of the plant and the lump disturbances at each time step k. Then, the error state is returned to the nominal state; the nominal state will be harnessed by the controller.

B. IMU Model of ESESO

Given the IMU measurements, we first write out the nominal state propagation in discrete time of $\mathbf{z}$;

$$\mathbf{z}_k = \mathbf{f}(\mathbf{z}_{k-1}, \mathbf{u}_k) \tag{10a}$$

$$\begin{cases} \mathbf{p}_k = \mathbf{p}_{k-1} + \mathbf{v}\Delta t + \frac{1}{2}(\mathbf{R}_\Theta(\mathbf{u}_a - \mathbf{b}_a) + \mathbf{g}_\mathcal{I})\Delta t^2 \\ \mathbf{v}_k = \mathbf{v}_{k-1} + (\mathbf{R}_\Theta(\mathbf{u}_a - \mathbf{b}_a) + \mathbf{g}_\mathcal{I})\Delta t \\ \mathbf{R}_{\Theta,k} = \mathbf{R}_{\Theta,k-1}\mathbf{Exp}((\mathbf{u}_g - \mathbf{b}_g)\Delta t) \\ \mathbf{b}_{g,k} = \mathbf{b}_{g,k-1} \\ \mathbf{b}_{a,k} = \mathbf{b}_{a,k-1} \\ \mathbf{g}_{\mathcal{I},k} = \mathbf{g}_{\mathcal{I},k-1} \\ \boldsymbol{\xi}_k = \boldsymbol{\xi}_{k-1} \end{cases}, \tag{10b}$$

where Δt is the time difference between time step $k-1$ and k. Note that the IMU measurement is denoted as $\mathbf{u} = [\mathbf{u}_a, \mathbf{u}_g]^\top$ with $\mathbf{u}_a$ and $\mathbf{u}_g$ be the accelerometer and gyroscope measurement, respectively. Using Eqs. (9) and (10), the error state dynamics can be yielded as

$$\delta\mathbf{z}_k = \mathbf{f}_\delta(\delta\mathbf{z}_{k-1}, \mathbf{u}_k, \mathbf{w}) \tag{11a}$$

$$\begin{cases} \delta\mathbf{p}_k = \delta\mathbf{p}_{k-1} + \delta\mathbf{v}_k\Delta t \\ \delta\mathbf{v}_k = \mathbf{v}_{k-1} + ([-\mathbf{R}_\Theta(\mathbf{u}_a - \mathbf{b}_a)]_\times\delta\mathbf{R}_\Theta - \mathbf{R}_\Theta\delta\mathbf{b}_a + \delta\mathbf{g}_\mathcal{I})\Delta t + \mathbf{w}_\mathbf{v} \\ \delta\mathbf{R}_{\Theta,k} = \mathbf{Exp}(-(\mathbf{u}_g - \mathbf{b}_g)\Delta t)\delta\mathbf{R}_{\Theta,k-1} - \delta\mathbf{b}_g\Delta t + \mathbf{w}_\mathbf{R} \\ \delta\mathbf{b}_{g,k} = \delta\mathbf{b}_{g,k-1} + \mathbf{w}_{\mathbf{b}_a} \\ \delta\mathbf{b}_{a,k} = \delta\mathbf{b}_{a,k-1} + \mathbf{w}_{\mathbf{v}_g} \\ \delta\mathbf{g}_{\mathcal{I},k} = \delta\mathbf{g}_{\mathcal{I},k-1} \\ \delta\boldsymbol{\xi}_k = \delta\boldsymbol{\xi}_{k-1} + \mathbf{w}_{\boldsymbol{\xi}} \end{cases} \tag{11b}$$

The $\mathbf{w}$ is the process noise. Further, there is

$$\delta\mathbf{z}_k = \mathbf{f}_\delta(\delta\mathbf{z}_{k-1}) + \nabla\mathbf{f}\delta\mathbf{z}_k + \mathbf{w}, \tag{12}$$

where $\nabla\mathbf{f} = \frac{\partial\mathbf{f}_\delta}{\partial\delta\mathbf{z}}$ is equivalent to the Jacobian matrix of $\mathbf{f}_\delta(\cdot)$. Recall that the mean of the error state is $\mathbf{0}$, making $\mathbf{f}(\delta\mathbf{z}_k) = \mathbf{0}$. We can then propagate the covariance matrix of last time-step with $\nabla\mathbf{f}$. Therefore, the prediction step of the ESESO is given by:

$$\check{\delta\mathbf{z}}_k = \nabla\mathbf{f}\delta\hat{\mathbf{z}}_{k-1} \tag{13a}$$

$$\check{\mathbf{P}}_k = \nabla\mathbf{f}_k\hat{\mathbf{P}}_{k-1}\nabla\mathbf{f}_k^\top + \mathbf{Q}, \tag{13b}$$

where $\mathbf{Q}$ is a diagonal matrix based on the processing noise $\mathbf{w}$.

C. Update Model of ESESO

An abstract sensor is needed to observe the error state for the ESESO. In this work, we opted for a simulated GPS/GNSS and the thrust measurement to perform the update of the filter. The sensor model is defined as,

$$\mathbf{y}_k = \mathbf{h}(\mathbf{z}_k) + \boldsymbol{\zeta} \tag{14a}$$

$$\begin{cases} \mathbf{p}_{k,\text{GPS}} = \mathbf{p}_k + \boldsymbol{\zeta}_\mathbf{p} \\ \mathbf{v}_{k,\text{GPS}} = \dot{\mathbf{p}}_{k,\text{GPS}} + \boldsymbol{\zeta}_\mathbf{v} \\ \mathbf{R}_{\Theta,k,\text{GPS}} = \mathbf{R}_{\Theta,k}\mathbf{Exp}(\boldsymbol{\zeta}_{\mathbf{R}_\Theta}) \\ \boldsymbol{\tau}_k = \mathbf{h}_\tau(\mathbf{x}_k) + \boldsymbol{\zeta}_{\boldsymbol{\tau}} \end{cases} \tag{14b}$$

where

$$\begin{aligned}\mathbf{h}_\tau(\mathbf{x}) = \mathbf{M}_{RB}(\mathbf{u}_a - \mathbf{b}_a) + \mathbf{M}_A(\mathbf{u}_a - \mathbf{b}_a + \mathbf{R}_\Theta^\top\mathbf{g}_\mathcal{I}) \\ + \mathbf{D}(\mathbf{R}_\Theta^\top\mathbf{v})\mathbf{R}_\Theta^\top\mathbf{v} + \mathbf{R}_\Theta^\top\mathbf{g}(\mathbf{R}_\Theta) - \boldsymbol{\xi}\end{aligned}$$

$\boldsymbol{\zeta} = \left[\boldsymbol{\zeta}_\mathbf{p}^\top, \boldsymbol{\zeta}_\mathbf{v}^\top, \boldsymbol{\zeta}_{\mathbf{R}_\Theta}^\top, \boldsymbol{\zeta}_{\boldsymbol{\tau}}^\top\right]^\top \in \mathbb{R}^{12}$ is the measurement noise.

Remark 1: We omit the Coriolis and centripetal force, as the rotational velocities are relatively small, making the term negligible. Also note that the raw velocity measurement $\mathbf{v}_{k,\text{GPS}}$ is acquired by numerical differentiation.

The Jacobian matrix of the measurement model can be derived as

$$\nabla\mathbf{h}_k = \frac{\partial\mathbf{h}}{\partial\mathbf{z}}\frac{\partial\mathbf{z}}{\partial\delta\mathbf{z}}. \tag{15}$$

To fix the non-differentiable quadratic term as shown in Eq. (3), $\mathbf{D}_A$ is approximated with a polynomial fitting function

$$\mathbf{D}_A(\mathbf{v})\mathbf{v} = -\text{diag}[\mathbf{d}_{NL} \circ |\mathbf{v}|]\mathbf{v} \simeq \mathbf{p}_{\mathbf{D}}(\mathbf{v})$$

The updated equations are then given by

$$\mathbf{K}_k = \check{\mathbf{P}}_k \nabla \mathbf{h}_k (\nabla \mathbf{h}_k \check{\mathbf{P}}_k \nabla \mathbf{h}_k^\top + \mathbf{R})^{-1} \tag{16a}$$

$$\delta \hat{\mathbf{z}}_k = \mathbf{K}_k (\mathbf{y}_k \boxminus \mathbf{h}(\mathbf{z}_k)) \tag{16b}$$

$$\hat{\mathbf{P}}_k = (\mathbf{I} - \mathbf{K}_k \nabla \mathbf{h}_k) \check{\mathbf{P}}_k \tag{16c}$$

$$\hat{\mathbf{z}}_k = \mathbf{z}_k \boxplus \delta \mathbf{z}_k, \tag{16d}$$

$\mathbf{R}$ is the diagnal matrix based on the measurement noise $\boldsymbol{\zeta}$. Note that Eq. (16d) is the final update process, which is referred to as error injection. After the update step, we then set the error back to $\mathbf{0}$ for the next time step:

$$\delta \hat{\mathbf{z}}_k := \mathbf{0} \tag{17a}$$

$$\hat{\mathbf{P}}_k := \nabla \mathbf{j} \hat{\mathbf{P}}_k \nabla \mathbf{j}^\top, \tag{17b}$$

where $\nabla \mathbf{j}$ is the Jacobian matrix of the reset function

$$\mathbf{j}(\delta \mathbf{z}_k) = \delta \mathbf{z}_k \boxminus \delta \hat{\mathbf{z}}_k. \tag{18}$$

D. Stability Analysis

Note that the asymptotic stability of the EKF can be guaranteed in a Lyapunov sense [22]. Nevertheless, as we are tracking the error state in ESESO, the stability of the proposed observer has to be analyzed to the error dynamics of the error state. Using Eqs. (12), (15) and (16), the observe error dynamics can be given by

$$\begin{aligned} \boldsymbol{\epsilon}_k &= \delta \mathbf{z}_k - \delta \hat{\mathbf{z}}_k \\ \boldsymbol{\epsilon}_{k+1} &= \nabla \mathbf{f}_k (\mathbf{I} - \mathbf{K}_k \nabla \mathbf{h}_k) \boldsymbol{\epsilon}_k + \mathbf{r}_k, \end{aligned} \tag{19}$$

The matrices presented here are identical to the ones derived in Eqs. (12), (15) and (16). Meanwhile, from Eqs. (11a), (15), and (16a), it can be seen that both $\mathbf{f}_\delta(\cdot)$ and $\mathbf{h}_\delta(\cdot)$ are $\mathcal{C}_1$ functions, and $\mathbf{r}_k$ represents the higher order term (H.O.T.) of them.

A technical Lemma can be given as follows to guarantee the stability of the observing system.

Lemma 1: For observed error dynamics given by (19), the system is asymptotically stable if the following five conditions hold:

1) There exists $\bar{f}$, $\bar{h}$, $\bar{p}$, $\underline{p} \in \mathbb{R}^+$, s.t. $\forall k \geq 0$
$$\begin{aligned} \|\nabla \mathbf{f}_k\| \leq \bar{f}, \|\nabla \mathbf{h}_k\| \leq \bar{h} \\ \underline{p}\mathbf{I} \leq \check{\mathbf{P}}_k \leq \bar{p}\mathbf{I}, \underline{p}\mathbf{I} \leq \hat{\mathbf{P}}_k \leq \bar{p}\mathbf{I} \end{aligned}$$
2) $\forall k \geq 0$ rank$(\mathbf{F}_k) = n$.
3) Define the H.O.T. $\mathbf{r}_k$ of $\boldsymbol{\epsilon}_{k+1}$ as $\mathbf{r}_F + \mathbf{r}_H$, which are the respective H.O.T.s related to prediction and update models. There exists α, β_F, β_H, $\beta \in \mathbb{R} > 0$ s. t.
$$\begin{aligned} \|\mathbf{r}_F(\delta \mathbf{z}, \delta \hat{\mathbf{z}})\| &\leq \beta_F \|\delta \mathbf{z} - \delta \hat{\mathbf{z}}\|^2 \\ \|\mathbf{r}_H(\delta \mathbf{z}, \delta \check{\mathbf{z}})\| &\leq \beta_H \|\delta \mathbf{z} - \delta \check{\mathbf{z}}\|^2 \\ \|\mathbf{r}\| &\leq \beta \|\delta \mathbf{z} - \delta \check{\mathbf{z}}\|^2 \\ \|\delta \mathbf{z} - \delta \hat{\mathbf{z}}\| &\leq \alpha \\ \|\delta \mathbf{z} - \delta \check{\mathbf{z}}\| &\leq \alpha \end{aligned}$$
4) $\nabla \mathbf{f}_k$, $\nabla \mathbf{h}_k$ is assumed to satisfy the uniform observability condition.
5) $\mathbf{Q}$, $\mathbf{R}$ is symmetric positive definite.

The proof of condition 3) is supported by Lemma 4 in [23] and is omitted here.

Proof: The Lyapunov function is selected as

$$V_k(\boldsymbol{\epsilon}_k) = \boldsymbol{\epsilon}_k^\top \check{\mathbf{P}}_k^{-1} \boldsymbol{\epsilon}_k, \tag{20}$$

and with condition 1), we have

$$\frac{1}{\bar{p}} \|\boldsymbol{\epsilon}_k\|^2 \leq V_k(\boldsymbol{\epsilon}_k) \leq \frac{1}{\underline{p}} \|\boldsymbol{\epsilon}_k\|^2. \tag{21}$$

$V_k(\boldsymbol{\epsilon}_k)$ is therefore positive definite and decrescent.

Using condition 2), 4), Eq. (16) and matrix inversion lemma [24], [25] yields

$$\begin{aligned} V_{k+1}(\boldsymbol{\epsilon}_{k+1}) &= \boldsymbol{\epsilon}_{k+1}^\top \check{\mathbf{P}}_{k+1}^{-1} \boldsymbol{\epsilon}_{k+1} \\ &\leq \boldsymbol{\epsilon}_k^\top [\check{\mathbf{P}}_k^{-1} - \check{\mathbf{P}}_k^{-1} (\hat{\mathbf{P}}_k^{-1} + \nabla \mathbf{f}_k^\top \mathbf{Q}^{-1} \nabla \mathbf{f}_k) \check{\mathbf{P}}_k^{-1}] \boldsymbol{\epsilon}_k \\ &\quad + 2\mathbf{r}_k^\top \check{\mathbf{P}}_{k+1}^{-1} \nabla \mathbf{f}_k (\mathbf{I} - \mathbf{K}_k \nabla \mathbf{h}_k) \boldsymbol{\epsilon}_k + \mathbf{r}_k^\top \check{\mathbf{P}}_{k+1}^{-1} \mathbf{r}_k \end{aligned} \tag{22}$$

$\mathbf{K}_k$ is also equivalent to $\hat{\mathbf{P}}_k \nabla \mathbf{h}_k^\top \mathbf{R}^{-1}$ from Eq. (16), and

$$\|\mathbf{K}_k\| \leq \left\| \hat{\mathbf{P}}_k \right\| \left\| \nabla \mathbf{h}_k^\top \right\| \left\| \mathbf{R}^{-1} \right\| \leq \frac{\bar{p}\bar{h}}{\underline{r}}. \tag{23}$$

$\underline{r}$ is $\lambda_{\min}$ of $\mathbf{R}$. Using conditions 1) and 3), Eq. (22), we have

$$\begin{aligned} V_{k+1}(\boldsymbol{\epsilon}_{k+1}) &\leq \boldsymbol{\epsilon}_k^\top \check{\mathbf{P}}_k^{-1} \boldsymbol{\epsilon}_k - \frac{1}{\bar{p}^2(\bar{p} + \bar{f}^2 \underline{q}^{-1})} \|\boldsymbol{\epsilon}_k\|^2 \\ &\quad + 2\beta \|\boldsymbol{\epsilon}_k\|^2 \bar{f} \|\boldsymbol{\epsilon}_k\| \frac{(1 + \bar{p}\bar{h}^2 \underline{r}^{-1})}{\underline{p}} \\ &\quad + \beta \|\boldsymbol{\epsilon}_k\|^2 \frac{1}{\underline{p}} \beta \|\boldsymbol{\epsilon}_k\| \alpha \end{aligned} \tag{24}$$

$$\begin{aligned} &= V_k(\boldsymbol{\epsilon}_k) - \{ \frac{1}{\bar{p}^2(\bar{p} + \bar{f}^2 \underline{q}^{-1})} \\ &\quad - (2\beta \bar{f} \frac{(1 + \bar{p}\bar{h}^2 \underline{r}^{-1})}{\underline{p}} + \beta^2 \frac{1}{\underline{p}} \alpha) \|\boldsymbol{\epsilon}_k\| \} \|\boldsymbol{\epsilon}_k\|^2. \end{aligned} \tag{25}$$

Further, there is

$$\begin{aligned} V_{k+1}(\boldsymbol{\epsilon}_{k+1}) &\leq V_k(\boldsymbol{\epsilon}_k) - \left\{ \frac{1}{\bar{p}^2(\bar{p} + \bar{f}^2 \underline{q}^{-1})} \right. \\ &\quad \left. - \left[2\beta \bar{f} \frac{(1 + \bar{p}\bar{h}^2 \underline{r}^{-1})}{\underline{p}} + \beta^2 \frac{1}{\underline{p}} \alpha \right] \|\boldsymbol{\epsilon}_k\| \right\} \|\boldsymbol{\epsilon}_k\|^2 \\ &= V_k(\boldsymbol{\epsilon}_k) - \left[\frac{1}{\bar{p}^2(\bar{p} + \bar{f}^2 \underline{q}^{-1})} - \mu \|\boldsymbol{\epsilon}_k\| \right] \|\boldsymbol{\epsilon}_k\|^2, \end{aligned} \tag{26}$$

where $\mu = 2\beta \bar{f} \frac{(1 + \bar{p}\bar{h}^2 \underline{r}^{-1})}{\underline{p}} + \beta^2 \frac{1}{\underline{p}} \alpha \geq 0$. Let $\alpha \leq \frac{1}{\bar{p}^2(\bar{p} + \bar{f}^2 \underline{q}^{-1})\mu}$, then $V_{k+1}(\boldsymbol{\epsilon}_{k+1}) - V_k(\boldsymbol{\epsilon}_k) \leq 0$. The proof is completed. ■

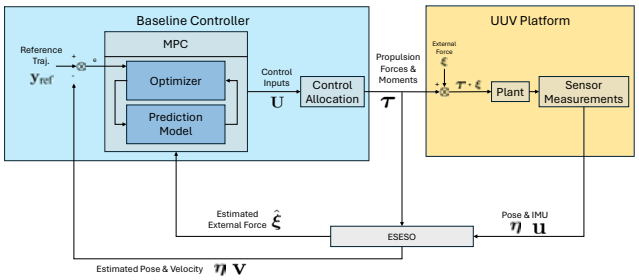

Fig. 1: Block diagram of the proposed adaptive MPC scheme for the UUV.

IV. Adaptive Model Predictive Control

A. Adaptive Prediction Model

Figure (1) illustrates the basic principle of the proposed adaptive MPC framework.

The dynamics model sent into the adaptive MPC framework can be given by

$$\begin{cases} \dot{\mathbf{p}} = \mathbf{v} \\ \dot{\mathbf{v}} = \mathbf{R}_\Theta \mathbf{M}^{-1}(\mathbf{K}_T \mathbf{A}\mathbf{U} - \mathbf{D}(\mathbf{v})\mathbf{v} - \mathbf{g}(\mathbf{R}_\Theta) + \boldsymbol{\xi}) \\ \dot{\psi} = s(\boldsymbol{\eta}_\mathcal{I}, \mathbf{v}_\mathcal{B}, \boldsymbol{\omega}_\mathcal{B})_\psi + U_\psi, \end{cases} \tag{27}$$

where the state is denoted as $\bar{\mathbf{x}} = [\mathbf{p}, \mathbf{v}, \psi]^\top$ and control input is $\mathbf{U} = [\mathbf{U}_T, U_\psi] \in \mathbb{R}^4$.

Remark 2: The MPC proposed here does not track the rotational velocity, while the rotational disturbances are also neglected. The scalar term $s(\boldsymbol{\eta}_\mathcal{I}, \mathbf{v}_\mathcal{B}, \boldsymbol{\omega}_\mathcal{B})_\psi$ is derived from Eq. (1) without considering the Coriolis and centripetal forces, where the rotational velocities are retrieved directly from IMU measurements and bias state $\omega_\mathcal{B} = \mathbf{u}_g - \mathbf{b}_g$. $\mathbf{K}_T \in \mathbb{R}^{6\times 3}$ is extracted from the propulsion matrix $\mathbf{K}$.

Remark 3: The adaptability is reflected within in Eq. (27), where the estimated lump disturbance is injected into the prediction model.

B. MPC Implementation

The MPC optimization problem can be expressed as

$$\begin{aligned} &\min_{\mathbf{U}} J = \sum_{k=T_0}^{T_{N-1}} \left[\|\mathbf{e}_k\|^2_{\mathbf{Q}_c} + \|\mathbf{U}_k\|^2_{\mathbf{R}_c} \right] + \|\mathbf{e}_{T_N}\|_{\mathbf{Q}_N}, \\ &\text{s.t. } \mathbf{e}_k = \mathbf{y}(\bar{\mathbf{x}}_k, \mathbf{U}_k) - \mathbf{r}_k \\ &\quad \mathbf{U}_k \in \mathcal{U}, \quad \bar{\mathbf{x}}_k \in \mathcal{X}, \quad \bar{\mathbf{x}}_{T_N} \in \mathcal{X}_N, \end{aligned} \tag{28}$$

where $\bar{\mathbf{x}}(t)$ and $\mathbf{U}(t)$ respectively denote the state and the control inputs, t_0 and t_N are the first and last time-steps of control horizon, and $\mathbf{r}(t)$ is the reference state. Furthermore, $\mathbf{y}(\cdot)$ represents the system integration output based on the dynamic model defined in Eq. (27). $\mathbf{Q}_c$, $\mathbf{R}_c$, and $\mathbf{Q}_N$ are the weighting matrices, $\mathcal{U}$, $\mathcal{X}$, and $\mathcal{X}_N$ are the input, state, and terminal constraint sets. Note that $\mathbf{Q}_c, \mathbf{R}_c, \mathbf{Q}_N \succ 0$.

Via multiple shooting method, the above problem at $t = k$ is then reformulated as

$$\begin{aligned} &\min_{\bar{\mathbf{x}}, \mathbf{U}} J_k = \sum_{i=k}^{k+N-1} l(\bar{\mathbf{x}}_i, \mathbf{U}_i) + l_f(\bar{\mathbf{x}}_{k+N}, \mathbf{U}_{k+N}), \\ &\text{s.t. } \mathbf{U}_i \in \mathcal{U}, \quad \bar{\mathbf{x}}_i \in \mathcal{X}, \quad \bar{\mathbf{x}}_{t_N} \in \mathcal{X}_N, \end{aligned} \tag{29}$$

where $l(\cdot)$ and $l_f(\cdot)$ are the positive definite functions that are respectively related to the stage and the terminal cost. Here we utilize ACADOS [26] to solve the MPC in real-time.

C. Stability Analysis

A stability lemma is given as the following to show the stability of the controller. First, an assumption on the terminal cost and constraint is made.

Assumption 1: For all $\bar{\mathbf{x}} \in \mathcal{X}_N$, the terminal cost $l_f(\cdot)$ is a continuous Lyapunov function such that

$$l_f(\mathbf{y}(\bar{\mathbf{x}}, \mathbf{U})) - l_f(\bar{\mathbf{x}}, \mathbf{U}) \leq -l(\bar{\mathbf{x}}, \mathbf{U}). \tag{30}$$

Based on Assumption 1, the lemma is given as follows.

Lemma 2: With the optimization problem defined in Eq. (28), the MPC controller is asymptotically stable if the following conditions hold:

1) $\mathcal{U}, \mathcal{X}, \mathcal{X}_N \neq \emptyset$.
2) Only the $\mathbf{U}(k)$ is inputted to the system.
3) N is sufficiently large and global optimal can be acquired at each time k.
4) $J_k = 0$ if $\bar{\mathbf{x}}, \mathbf{U} = 0$.
5) The prediction model is unbiased and has no measurement noises.
6) Assumption 1 holds.

Proof: Define Lyapunov function as $V_k = \min J_k$, there is

$$V_k = \sum_{i=k}^{k+N-1} l(\bar{\mathbf{x}}_i, \mathbf{U}_i) + l_f(\bar{\mathbf{x}}_{k+N}, \mathbf{U}_{k+N}) \tag{31}$$

Obviously, V_k is positive definite. Similarly,

$$\begin{aligned} V_{k+1} &= \sum_{i=k+1}^{k+N} l(\bar{\mathbf{x}}_i, \mathbf{U}_i) + l_f(\bar{\mathbf{x}}_{k+1+N}, \mathbf{U}_{k+1+N}) \\ &= \sum_{i=k}^{k+N-1} l(\bar{\mathbf{x}}_i, \mathbf{U}_i) + l_f(\bar{\mathbf{x}}_{k+N}, \mathbf{U}_{k+N}) \\ &\quad + l_f(\bar{\mathbf{x}}_{k+1+N}, \mathbf{U}_{k+1+N}) - l(\bar{\mathbf{x}}_k, \mathbf{U}_k) \\ &\quad - l_f(\bar{\mathbf{x}}_{k+N}, \mathbf{U}_{k+N}) + l(\bar{\mathbf{x}}_{k+N}, \mathbf{U}_{k+N}) \end{aligned} \tag{32}$$

Using condition 6) and Lemma 2 in Eq. (31) yields

$$\begin{aligned} V_{k+1} = V_k &- l(\bar{\mathbf{x}}_k, \mathbf{U}_k) + l_f(\bar{\mathbf{x}}_{k+1+N}, \mathbf{U}_{k+1+N}) \\ &- l_f(\bar{\mathbf{x}}_{k+N}, \mathbf{U}_{k+N}) + l(\bar{\mathbf{x}}_{k+N}, \mathbf{U}_{k+N}) \end{aligned} \tag{33}$$

Using the facts that

$$-l(\bar{\mathbf{x}}_{k+1}, \mathbf{U}_k) \leq 0$$

and

$$l_f(\bar{\mathbf{x}}_{k+1+N}, \mathbf{U}_{k+1+N}) - l_f(\bar{\mathbf{x}}_{k+N}, \mathbf{U}_{k+N}) + l(\bar{\mathbf{x}}_{k+N}, \mathbf{U}_{k+N}) \leq 0,$$

The difference equation of V_k is semi-negative definite. The proof is completed. ■

V. Semi-physical Simulation Results

The simulation results are implemented in ROS Gazebo SITL with a BlueROV2 model[27]. Table I lists some parameters of virtual sensors and controllers.

TABLE I: Simulation parameters.

Parameters	Value
IMU frequency	50 Hz
GPS frequency	30 Hz
$\mathbf{Q}$	$0.001\mathbf{I}$
$\mathbf{R}$	diag[$0.01\mathbf{I}$ $0.02\mathbf{I}$ $0.0006\mathbf{I}$ $0.012\mathbf{I}$]
Controller frequency	20
Prediction horizon	80
$\mathbf{Q}_c$	[300 300 150 10 10 150 10 10 10 10 10 10]
$\mathbf{R}_c$	[1 1 1 0.5]
m	11.26 kg
$\mathbf{m}$	[1.7182 0 5.468 kg 0 1.2481 0.4006 0 kgm^2/rad]
W	112.8 N
B	114.8 N
z_{CG}	0.2 m
$\mathbf{I}$	[0.3 0.63 0.58] kgm^2
$\mathbf{d}_L$	[-11.7391 Ns/m -20 Ns/m -31.8678 Ns/m -25 Ns/rad -44.9085 Ns/rad -5 Ns/rad]
$\mathbf{d}_{NL}$	[-18.18 Ns/m -21.66 Ns/m -36.99 Ns/m -1.55 Ns/rad -1.55 Ns/rad -1.55 Ns/rad]

To validate the effectiveness of the proposed observer and the adaptive controller, we present the results of both state estimation and trajectory tracking. Figure 2 presents the pose estimation results, while figure 3 showcases the velocity and the estimated disturbance.

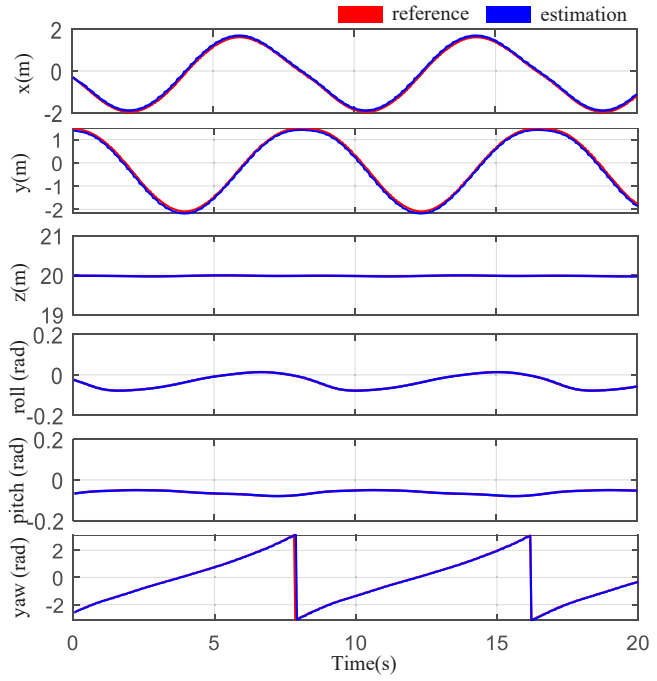

Fig. 2: The estimated pose versus the ground truth from the ESESO.

In Figure 2, the pose and the velocity ground truth are retrieved directly from the Gazebo software, whereas the ground truth of the disturbance is generated artificially based on the ideal dynamic model presented in Eq. (1). Figures 2 and 3 indicate that the state converges to the ground truth, providing an accurate estimation of the robot state and the lump disturbance for the controller.

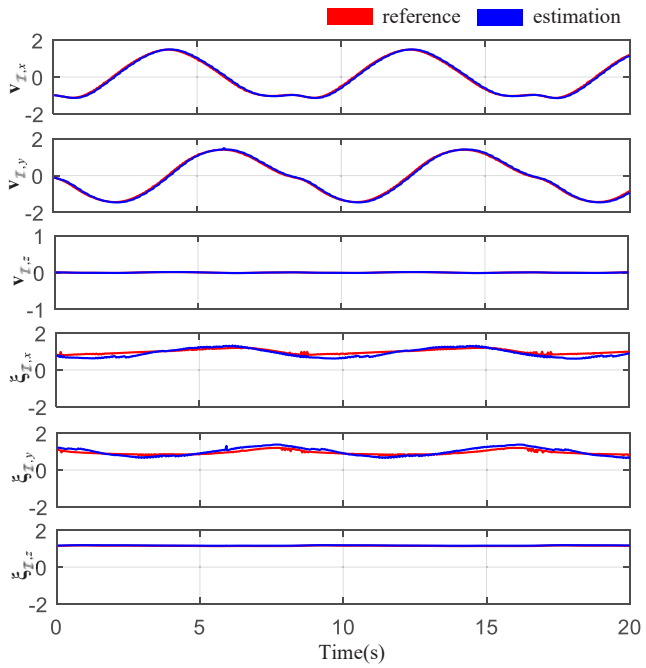

Fig. 3: The estimated velocity and disturbance versus the ground truth from the ESESO.

To validate the superiority of the proposed ESESO-AMPC framework, a circular path with an external disturbance of $[40N, 40N, 10N]$ is given as the reference signal of the UUV. Figure 4 records the tracking performance under different control frameworks. The blue curve in Figure 4 indicates that the proposed ESESO-AMPC framework outperforms the others. Additionally, the tracking errors are also illustrated in Figure 5. It is obvious to validate that NLMPC and PID have greater errors without disturbance observers.

VI. Conclusions

In this paper, a novel ESESO-AMPC framework is proposed to address UUV control problem subject to external disturbances and measurement noise. The ESESO is conducted as a disturbance compensator of the AMPC framework. In contrast to other works, the observing scheme proposed in this paper can simultaneously estimate the lump disturbances and can be applied to sensor fusion problems. Additionally, all simulation experiments are conducted in a semi-physical experiment so that the proposed method can be directly transferred to real UUVs. The stability of both the observing and control systems is analyzed in a Lyapunov sense. Sufficient simulations are implemented to verify the effectiveness, robustness, and superiority of the proposed control framework. Our future work will focus on addressing the control problem of UUVs with model uncertainties and severe wave disturbances with other sensor models.

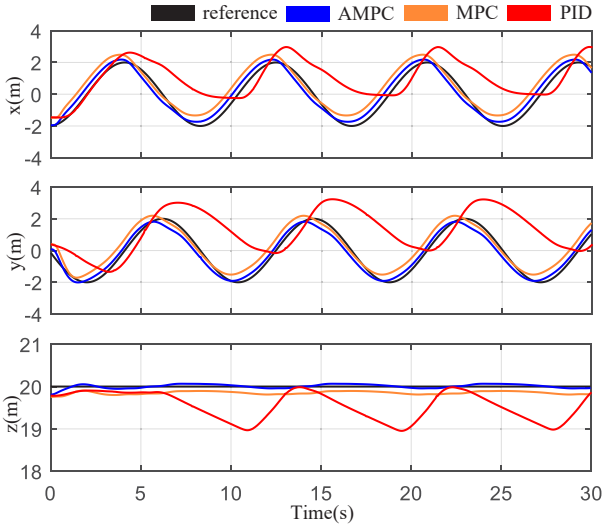

Fig. 4: The control performance of AMPC, MPC and PID.

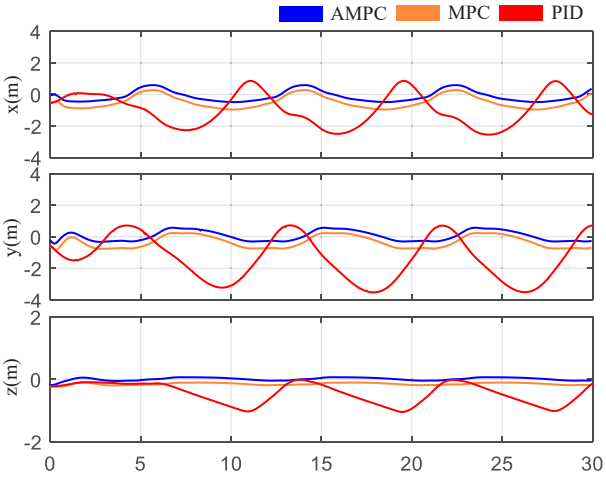

Fig. 5: The tracking error of adaptive AMPC, MPC and PID.

REFERENCES

[1] C. Lin, Y. Cheng, X. Wang, J. Yuan, and G. Wang, "Transformer-based dual-channel self-attention for uuv autonomous collision avoidance," *IEEE Transactions on Intelligent Vehicles*, vol. 8, no. 3, pp. 2319–2331, 2023.

[2] J. Wang, F. Chen, Y. Huang, J. McConnell, T. Shan, and B. Englot, "Virtual maps for autonomous exploration of cluttered underwater environments," *IEEE Journal of Oceanic Engineering*, vol. 47, no. 4, pp. 916–935, 2022.

[3] S. Hu, R. Feng, Z. Wang, C. Zhu, Z. Wang, Y. Chen, and H. Huang, "Control system of the autonomous underwater helicopter for pipeline inspection," *Ocean Engineering*, vol. 266, p. 113190, 2022.

[4] S. Hou, D. Jiao, B. Dong, H. Wang, and G. Wu, "Underwater inspection of bridge substructures using sonar and deep convolutional network," *Advanced Engineering Informatics*, vol. 52, p. 101545, 2022.

[5] X. Cao, C. Sun, and X. Wang, "Threat assessment strategy of human-in-the-loop unmanned underwater vehicle under uncertain events," *IEEE Transactions on Systems, Man, and Cybernetics: Systems*, 2023.

[6] M. J. Er, H. Gong, Y. Liu, and T. Liu, "Intelligent trajectory tracking and formation control of underactuated autonomous underwater vehicles: A critical review," *IEEE Transactions on Systems, Man, and Cybernetics: Systems*, vol. 54, no. 1, pp. 543–555, 2024.

[7] H.-S. Jin, H. Cho, H. Jiafeng, J.-H. Lee, M.-J. Kim, S.-K. Jeong, D.-H. Ji, K. Joo, D. Jung, and H.-S. Choi, "Hovering control of uuv through underwater object detection based on deep learning," *Ocean Engineering*, vol. 253, p. 111321, 2022.

[8] H. Zhao and D. Zhu, "Uuv trajectory tracking control with fault tolerant based on mpc," in *2020 Chinese Control And Decision Conference (CCDC)*, 2020, pp. 2403–2408.

[9] W. Zhang, P. Han, Y. Liu, Y. Zhang, W. Wu, and Q. Wang, "Design of an improved adaptive slide controller in uuv dynamic base recovery," *Ocean Engineering*, vol. 285, p. 115266, 2023.

[10] C. P. E. Y. Huanca, G. P. Incremona, and P. Colaneri, "Design of a distributed switching model predictive control for quadrotor uavs aggregation," *IEEE Control Systems Letters*, vol. 7, pp. 2964–2969, 2023.

[11] M. Bahadorian, B. Savkovic, R. Eaton, and T. Hesketh, "Robust model predictive control for automated trajectory tracking of an unmanned ground vehicle," in *2012 American Control Conference (ACC)*. IEEE, 2012, pp. 4251–4256.

[12] H. Xie, L. Dai, Y. Lu, and Y. Xia, "Disturbance rejection mpc framework for input-affine nonlinear systems," *IEEE Transactions on Automatic Control*, vol. 67, no. 12, pp. 6595–6610, 2022.

[13] H. Xie, L. Dai, Y. Luo, and Y. Xia, "Robust mpc for disturbed nonlinear discrete-time systems via a composite self-triggered scheme," *Automatica*, vol. 127, p. 109499, 2021.

[14] T. Shi, P. Shi, and Z.-G. Wu, "Dynamic event-triggered asynchronous mpc of markovian jump systems with disturbances," *IEEE Transactions on Cybernetics*, vol. 52, no. 11, pp. 11 639–11 648, 2022.

[15] H. Zheng, Y. Sun, G. Zhang, L. Zhang, and W. Zhang, "Research on real time obstacle avoidance method for auv based on combination of vit-dpfn and mpc," *IEEE Transactions on Instrumentation and Measurement*, vol. 73, pp. 1–15, 2024.

[16] Y. Dai, S. Yu, and Y. Yan, "An adaptive ekf-fmpc for the trajectory tracking of uvms," *IEEE Journal of Oceanic Engineering*, vol. 45, no. 3, pp. 699–713, 2019.

[17] V. Madyastha, V. Ravindra, S. Mallikarjunan, and A. Goyal, "Extended kalman filter vs. error state kalman filter for aircraft attitude estimation," in *AIAA Guidance, Navigation, and Control Conference*, 2011, p. 6615.

[18] B. Robotics, "Bluerov2: The world's most affordable high-performance rov," *BlueROV2 Datasheet; Blue Robotics: Torrance, CA, USA*, 2016.

[19] T. I. Fossen, *Handbook of marine craft hydrodynamics and motion control*. John Wiley & Sons, 2011.

[20] S. Li, J. Yang, W.-H. Chen, and X. Chen, "Generalized extended state observer based control for systems with mismatched uncertainties," *IEEE Transactions on Industrial Electronics*, vol. 59, no. 12, pp. 4792–4802, 2011.

[21] H. Sun, R. Madonski, S. Li, Y. Zhang, and W. Xue, "Composite control design for systems with uncertainties and noise using combined extended state observer and kalman filter," *IEEE Transactions on Industrial Electronics*, vol. 69, no. 4, pp. 4119–4128, 2021.

[22] K. Reif and R. Unbehauen, "The extended kalman filter as an exponential observer for nonlinear systems," *IEEE Transactions on Signal processing*, vol. 47, no. 8, pp. 2324–2328, 1999.

[23] X.-Y. Kong and G.-H. Yang, "Secure state estimation for train-to-train communication systems: A neural network-aided robust ekf approach," *IEEE Transactions on Industrial Electronics*, pp. 1–11, 2024.

[24] J. Sherman, "Adjustment of an inverse matrix corresponding to changes in the elements of a given column or row of the original matrix," *Annu. Math. Statist.*, vol. 20, p. 621, 1949.

[25] M. A. Woodbury, *Inverting modified matrices*. Department of Statistics, Princeton University, 1950.

[26] R. Verschueren, G. Frison, D. Kouzoupis, J. Frey, N. v. Duijkeren, A. Zanelli, B. Novoselnik, T. Albin, R. Quirynen, and M. Diehl, "acados—a modular open-source framework for fast embedded optimal control," *Mathematical Programming Computation*, vol. 14, no. 1, pp. 147–183, 2022.

[27] M. M. M. Manhães, S. A. Scherer, M. Voss, L. R. Douat, and T. Rauschenbach, "Uuv simulator: A gazebo-based package for underwater intervention and multi-robot simulation," in *OCEANS 2016 MTS/IEEE Monterey*. Ieee, 2016, pp. 1–8.